Line centers, pressure shift, and pressure broadening of 1530–1560 nm hydrogen cyanide wavelength calibration lines

William C. Swann and Sarah L. Gilbert

Optoelectronics Division, National Institute of Standards and Technology, Boulder, Colorado 80305

Received December 1, 2004; revised manuscript received February 18, 2005; accepted January 11, 2005

We have measured the line centers and pressure-induced shift and broadening of 25 lines in the $2\nu_3$ rotational–vibrational band of hydrogen cyanide $H^{13}C^{14}N$. These lines can be used as wavelength references in the optical fiber communication wavelength division multiplexing *C*-band (approximately 1530–1565 nm). We find that the pressure shift varies with line number from +0.09 pm/kPa to −0.15 pm/kPa (approximately −1.5 to +2.5 MHz/Torr). The pressure broadening also varies with line number and is typically between 1 and 5.4 pm/kPa (17–90 MHz/Torr). We determined the line centers of 21 lines with an expanded uncertainty (2σ) of 0.01 pm (≈1 MHz), an improvement of more than 1 order of magnitude over previous line center measurements of this band. We also calculate the molecular constants for the band, yielding improved determination of the band origin frequency and the excited-state molecular constants.

OCIS codes: 020.3690, 060.2330, 120.3940, 120.4800, 300.1030, 300.6390.

1. INTRODUCTION

Wavelength division multiplexing (WDM) in optical fiber communication systems increases bandwidth by use of many wavelength channels. Current WDM systems typically employ 50 or 100 GHz channel spacing (0.4 or 0.8 nm, respectively) in the 1530–1565 nm WDM *C*-band. WDM will likely expand into the *L*-band region (approximately 1565–1625 nm), and WDM may be implemented in shorter-wavelength regions as well. Wavelength references are needed in these regions to calibrate instruments that are used to characterize components and monitor the wavelengths of the channels. In addition, optical fiber sensors based on the wavelength shift of fiber Bragg grating reflection peaks require wavelength calibration; some of these systems need wavelength calibration references with better than 1 pm uncertainty. These sensor systems typically operate in the optical fiber communication regions, particularly the WDM *C*-band, where components and measurement equipment are readily available.

Fundamental atomic or molecular absorptions provide wavelength references that are stable under changing environmental conditions such as temperature and pressure variations or the presence of electromagnetic fields. The National Institute of Standards and Technology (NIST) has developed wavelength calibration transfer standards in the 1510–1630 nm region based on acetylene,[1,2] hydrogen cyanide,[3] and carbon monoxide.[4,5] The hydrogen cyanide $H^{13}C^{14}N$ spectrum, shown in Fig. 1, is particularly well matched to the WDM *C*-band, with more than 50 strong absorption lines in the 1530–1565 nm region. We decided to upgrade the hydrogen cyanide NIST Standard Reference Material (SRM) transfer standard to higher accuracy. The vacuum wavelengths of lines in the hydrogen cyanide $H^{13}C^{14}N$ $2\nu_3$ rotational–vibrational band have been determined at very low pressure with an uncertainty of 0.12 pm (about 15 MHz).[6] Since we would like to certify our SRM to comparable or higher accuracy than this, we require improved accuracy on the line center values.

For a wavelength reference, the stability of the wavelength of each absorption line is a critical characteristic. The largest potential source of line shift is the energy-level shift caused by the interaction of the molecules during elastic collisions.[7] Commonly called the pressure shift, this shift depends linearly on the collision frequency. It is often desirable to use an intermediate or high-pressure sample for wavelength calibration of instruments, to pressure broaden the lines, and to match the reference bandwidth to the instrument resolution. This results in the strongest signals for a given resolution bandwidth. The hydrogen cyanide SRM will be at a pressure of 3.3 kPa (25 Torr). Thus we also need accurate measurements of the pressure shift of each line to determine the SRM wavelengths.

We measured the line centers, pressure shifts, and pressure broadening of 25 lines in the $2\nu_3$ rotational–vibrational band of hydrogen cyanide $H^{13}C^{14}N$. We also extrapolated these line centers to zero pressure and compared those values with the literature values. Finally, we determined the molecular constants for the band. We describe our measurement procedure in Section 2 and summarize the results in Section 3. Conclusions are presented in Section 4.

2. MEASUREMENT DESCRIPTION AND DATA ANALYSIS

A schematic diagram of our measurement apparatus is shown in Fig. 2. Light from a tunable diode laser is filtered using a fiber Fabry–Perot filter and is typically sent through two absorption cells simultaneously; the trans-

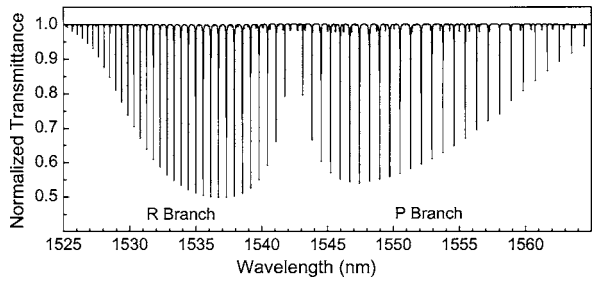

Fig. 1. Hydrogen cyanide $H^{13}C^{14}N$ $2\nu_3$ rotational–vibrational band spectrum obtained by scanning a tunable diode laser and measuring the laser power transmitted through a 15 cm long cell filled to a pressure of 3.3 kPa (25 Torr).

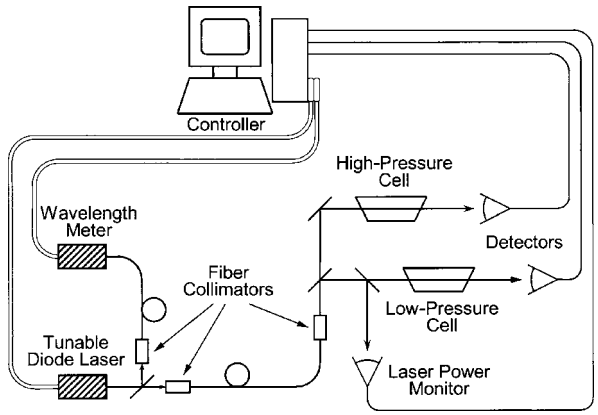

Fig. 2. Diagram of the pressure shift measurement apparatus.

mission through each cell is monitored by detectors. One cell contained $H^{13}C^{14}N$ gas at a relatively low pressure of $\approx$0.13 kPa (1 Torr), and the other contained a higher pressure of either 3.3 kPa (25 Torr) or 6.0 kPa (45 Torr). A third detector monitored the laser power, and a wavelength meter measured the laser's vacuum wavelength with a standard uncertainty (1σ) of $\approx$2.5 parts in 10^9 (0.5 MHz or 0.004 pm at 1560 nm). A computer controlled the laser wavelength scan and recorded the readings of the three detectors and wavelength meter.

The fused-silica absorption cells are 15 cm long, with windows attached to the cells by a glass frit method. To prevent interference fringes in the transmitted signal, the windows are mounted at an angle of 11° and are also wedged by $\approx$2°. The cells were first evacuated and leak checked and were then filled with isotopically pure gas. The $H^{13}C^{14}N$ gas was produced by reducing 99% isotopically pure potassium cyanide with stearic acid under vacuum and mild heat (approximately 80 °C). The reaction generates $H^{13}C^{14}N$ gas, a small amount of other isotopic species of hydrogen cyanide (HCN), traces of H_2O and CO_2 from decomposition of the stearic acid, and other reaction products that remain solid under vacuum. The gas sample was transferred from the reaction flask into a separate, previously evacuated flask. The trace of CO_2 gas was removed by freezing this flask in a dry ice bath, then opening the flask to a vacuum pump that pumps the CO_2 away from the frozen HCN. The HCN sample was then transferred to a flask containing phosphorous pentoxide desiccant that removes the trace of H_2O. The HCN sample is stored in this flask until ready for use; any traces of air that migrate into the flask through the valve are removed immediately prior to use by freezing the flask in liquid nitrogen and pumping away any remaining gases. During the fill process the pressure in the fill manifold (and hence the cell) was monitored with a capacitance manometer. The higher-pressure cells were prepared under our direction by an outside vendor; these were tipped off at the stem using a torch, forming an all-glass seal. The low-pressure cell was prepared in-house to allow further control of the gas sample purity; this cell was sealed using a glass valve with O-ring seals.

Figure 3 shows spectra of line $P16$ obtained at 0.9 and 3.3 kPa HCN pressure. The pressure broadening in the higher-pressure spectrum is obvious, and a small shift in the center wavelength is apparent. The measured quantity, the transmitted laser power I_T, is related to the absorption coefficient α and the absorption path length L by

$$I_T = I_0 \exp(-\alpha L), \tag{1}$$

where I_0 is the incident laser power. We first divided the cell transmission curves by the laser power monitor signal to remove common-mode intensity variations and normalized the data. We then took the natural logarithm to obtain the absorbance αL.

Individual lines were then fitted to Voigt profiles[7] using an orthogonal distance regression algorithm.[8] With the orthogonal distance regression, called either error-in-variables or total-least-squares regression, we obtain the model parameters by minimizing the sum of squares of the orthogonal distances from the model to the data points. The fitting program was able to account for a background slope and uncertainties in both x (wavelength) and y (transmitted laser power). A Voigt profile is a convolution of Lorentzian and Gaussian profiles; it results when there is a combination of Gaussian broadening (resulting from Doppler broadening, for example) and Lorentzian line shape (resulting from the natural linewidth or pressure broadening, for example). In our situation, the natural linewidth is small (typically $<$2 MHz for molecular absorption lines in this region[9]) compared with the Gaussian Doppler broadening ($\approx$450 MHz) and the Lorentzian pressure broadening. The pressure-broadened

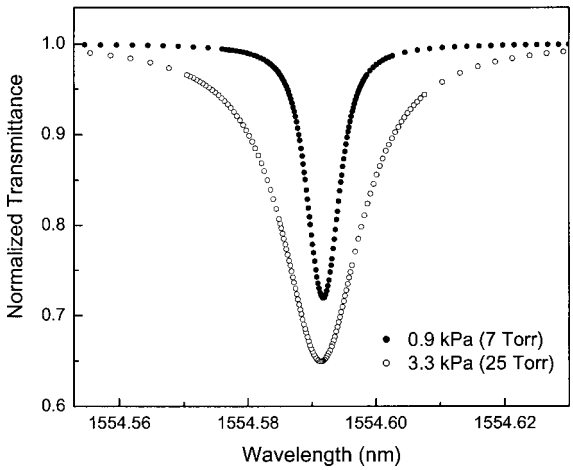

Fig. 3. Tunable diode laser scan of $H^{13}C^{14}N$ line $P16$ showing the transmittance through a low-pressure cell (0.9 kPa) and a higher-pressure (3.3 kPa) cell.

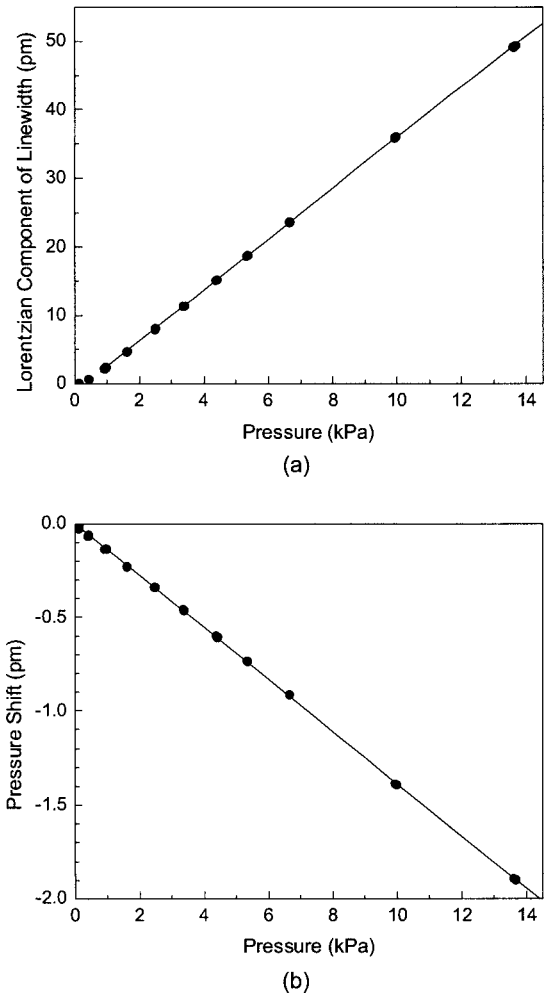

Fig. 4. (a) FWHM of the Lorentzian component of $H^{13}C^{14}N$ line $P16$ versus pressure and the corresponding linear least-squares fit to the higher-pressure data (>0.9 kPa). (b) Line $P16$ center wavelength shift from the zero-pressure value versus pressure and the corresponding linear least-squares fit to the data. For both plots, the error bars are smaller than the points.

component of the linewidths ranged from 0.04× to 9× the Doppler-broadened component. We used the calculated Doppler linewidth for each line, ranging from 3.57 to 3.62 pm (Ref. 7) and allowed the other fitting parameters to vary.

Short-term statistical variation of the wavelength meter reading and the laser power transmitted through the absorption cells added noise to the data scans. To determine this statistical variation of the wavelength measurement, we repeatedly measured the laser's wavelength while it was stabilized to a ^{87}Rb transition (see Subsection 2.A). The statistical variation of repeated measurements yielded a Gaussian distribution with a standard deviation of 0.004 pm. We determined the experimental uncertainty in the normalized transmitted laser power (transmittance) by measuring the statistical variation of the data within a region of a line wing. The standard deviation of these fluctuations was typically between 5×10^{-5} and 1×10^{-4}. To account for the short-term statistical variation, each data point of a scan was assigned a standard uncertainty of 0.004 pm for the wavelength and a fractional uncertainty of 1×10^{-4} for the transmittance. The fitting program determined the line centers and the Lorentzian component of the linewidths and the corresponding uncertainties. The resultant line-center-fit standard uncertainties were typically 0.003 pm.

To accurately determine the cells' pressures and monitor them over the course of the measurements, we generated a plot of the Lorentzian component of the linewidth (derived from the Voigt line fit) versus pressure for line $P16$. This allowed us to later determine a cell's pressure at any time by measuring the width of line $P16$ and comparing it with the plot. We mounted a cell in our pressure shift measurement apparatus and attached it to our fill manifold with a copper tube, which allowed us to monitor the cell pressure using the capacitance manometer while we measured the linewidth and line center. We conducted these measurements on line $P16$ for several pressures between 0.13 kPa (1 Torr) and 13 kPa (100 Torr). Figure 4(a) is a plot of the full width at half-maximum (FWHM) of the Lorentzian component of line $P16$ versus pressure. As can be seen, the Lorentzian component of the width (pressure broadening) has a linear dependence on pressure for pressures higher than ≈0.5 kPa. The deviation from this linear dependence at low pressure is likely due to collisional narrowing arising from velocity averaging. This effect is negligible at higher pressures, where pressure broadening dominates, but can cause the line shape to deviate from the expected Voigt profile at low pressures.[10] A linear least-squares fit to the higher-pressure data is also shown on the plot. Figure 4(b) shows the line center wavelength shift versus pressure for the same line and the corresponding linear least-squares fit; as can be seen from this plot, the pressure shift is linearly dependent on pressure. On the basis of our calibration of linewidth versus pressure for line $P16$, the pressures for the medium- and high-pressure cells used in the subsequent shift measurements were 3.36±0.02 kPa (25.22±0.13 Torr) and 5.91±0.03 kPa (44.34±0.22 Torr), respectively. The low-pressure cell, which was filled immediately prior to the measurements, showed an exponential decay in pressure from 0.133±0.008 kPa (1.00±0.06 Torr) to 0.106±0.008 kPa (0.80±0.06 Torr) over the nine-day duration of the measurements. This pressure change was likely due to adsorption of HCN on the cell surface; the pressure appeared to be approaching a steady-state value near 0.10 kPa. We did not observe any pressure change of the higher-pressure cells during the measurements. The pressure uncertainty quoted here is the expanded uncertainty obtained by applying a coverage factor of $k=2$ (i.e., our quoted uncertainty is $\pm2\sigma$).[11]

In Subsections 2.A and 2.B we discuss the aspects that contributed to our measurement uncertainty for the line center, pressure shift, and pressure-broadening measurements.

A. Wavelength Meter Uncertainty

We used a NIST-built wavelength meter that has a wavelength measurement standard deviation of 2.5 parts in 10^9 (equivalently, 0.004 pm, or 0.5 MHz at 1560 nm). We set up a high-accuracy wavelength reference to test the wavelength meter accuracy and statistical variation.[3] Diode laser light at 1560.5 nm is amplified with an erbium-

doped fiber amplifier and is frequency doubled in a periodically poled lithium niobate crystal. The resultant 780 nm light is then used to conduct saturated absorption spectroscopy on the $5S_{1/2} \rightarrow 5P_{3/2}$ transitions of rubidium (^{85}Rb and ^{87}Rb), and the laser is actively stabilized to one of the hyperfine components. The line centers of these transitions were measured with an uncertainty of ±0.4 MHz (Ref. 12), and the ^{87}Rb d/f crossover transition was measured with an uncertainty of 5.5 kHz.[13] We verified the accuracy of our stabilized laser by measuring its frequency with a stabilized frequency comb referenced simultaneously to the NIST calcium optical frequency standard and a hydrogen maser that was calibrated by the Cs clock.[14] Our measurement of the 1560 nm frequency with the laser stabilized to the ^{87}Rb d/f crossover transition is 192 113 990.7 MHz, with an expanded uncertainty (2σ) of ±0.7 MHz. This corresponds to the 780 nm frequency of 384 227 981.3 ± 1.4 MHz, which differs by only 0.6 MHz from the much more accurate determination of the ^{87}Rb d/f transition. We used this rubidium-stabilized reference to calibrate our wavelength meter between scans of the hydrogen cyanide lines; by averaging multiple measurements, we obtained a wavelength calibration standard uncertainty (1σ) of 0.35 MHz. We combined this wavelength calibration standard uncertainty with the uncertainty due to the wavelength meter drift between calibrations to obtain a wavelength measurement standard uncertainty of 0.004 pm (≈0.5 MHz) at 1560 nm. We verified the linearity of the wavelength meter by measuring a series of $^{12}C_2H_2$ lines between 1528 and 1538 nm. These measurements were performed much like our HCN line center measurements; the line centers for cells at two different pressures were measured, and the extrapolated zero-pressure line centers were compared with those reported in Ref. 9. We performed this measurement twice: once just before the HCN measurements and once near the completion of the HCN measurements. The average of our measured $^{12}C_2H_2$ line centers was within 0.002 pm of the values reported in Ref. 9, which have a standard uncertainty of 0.001 pm.

B. Background Variation

A slope or a variation in the background level can shift the apparent center of a line, particularly for the wide lines of the high-pressure cells. Interference fringes due to reflected laser light, wavelength dependence of the optical components, beam-pointing stability, and variations in the laser power can cause background variation. As mentioned above, we removed common-mode laser power variations by dividing the cell transmittance data by the power monitor data. To avoid effects due to the wavelength dependence of optical fiber couplers (splitters), we used free-space beam splitters to send the laser light to the cells and the power monitor. We minimized interference effects by using wedged cell windows and beam splitters, windowless detectors, and two optical isolators. These precautions reduced the background variation from these sources to a negligible level.

Wings of nearby absorption lines can also skew the shape of the line being measured and shift its apparent center. In addition to the strong lines of the $2\nu_3$ band, there are a number of weak lines throughout the spectrum that are due to hot bands (transitions that are not out of the ground vibrational state).[6] We also observed a number of weak $H^{12}C^{14}N$ and $H^{13}C^{15}N$ lines in our spectra; presumably these arise from incomplete separation of ^{12}C and a biasing toward the heavy isotope ^{15}N during the isotopic enrichment of the original potassium cyanide sample. To minimize the effect of weak neighboring lines on our line center and pressure shift measurements, we avoided measuring lines in the spectrum that had weak lines close to the primary line. To estimate the effect of weak nearby lines on the lines that we did measure, we developed a model in which we could add a weak line to a simulation of a particular measured line. The width and area of any weak lines within the flanks of a measured line were estimated by observing similar weak lines that were not adjacent to any strong lines. We obtained the offsets of any weak lines relative to a particular measured line from Ref. 6, which gives line centers for the hot-band transitions, as well as for the $H^{12}C^{14}N$ and $H^{13}C^{15}N$ lines. We then fitted the modeled line, both with and without the adjacent simulated weak line, using the same fitting routine we used to fit the measured lines. In both the data fitting and the simulation we limited the range of data being fit to the central portion of the line, clipping away any data with amplitude less than 35% of a line's maximum amplitude. Any weak lines outside of this data range were found to have a negligible effect on the simulated line centers; slopes in the fitted data caused by the wings of adjacent weak lines were accounted for by our fitting routine. Of all the lines we measured, only lines $R7$, $R8$, and $P20$ had adjacent weak lines with line centers within the fitted data; therefore we conclude that we can limit our detailed investigation to these lines. The line center difference given by the simulation's results with and without the weak line gives us an estimate of the line center shift caused by the adjacent weak line. The model showed negligible effects (shifts of less than 0.001 pm) of adjacent weak lines on the 0.13 kPa (1 Torr) line centers. Observation of the spectra verified this; the weak lines were clearly separated from the measured lines. The model revealed shifts of up to 0.005 pm for the 3.3 kPa (25 Torr) cell and up to 0.012 pm for the 6 kPa (45 Torr) cell. Extrapolating the modeled line centers to zero pressure revealed shifts as large as 0.004 pm for these lines.

3. PRESSURE SHIFT, LINE CENTER, AND PRESSURE-BROADENING RESULTS

The line center fit standard uncertainties for the 25 lines at three pressures were typically 0.003 pm. To obtain the unperturbed line center values, we extrapolated the line centers to zero pressure using a linear least-squares fitting procedure. We also derived the pressure shift coefficient (change in line center wavelength versus pressure) from this fit. The pressure-broadening coefficient for each line was determined by a linear least-squares fit to the Lorentzian component of the linewidth. We determined the uncertainties in these fit parameters using a Monte Carlo procedure whereby multiple least-squares fits to the data were performed within the boundaries of the data point uncertainties. The uncertainty in the respective fit parameters dominated the uncertainty of our pres-

Table 1. Line Center, Pressure Shift, and Pressure-Broadening Results for $H^{13}C^{14}N$[a]

Line	Line Center Extrapolated to Zero Pressure (vacuum wavelength, nm)	Shift Coefficient		Broadening Coefficient	
		(pm/kPa)	(MHz/Torr)	(pm/kPa)	(MHz/Torr)
*R*23	1528.926232(10)	0.060(2)	−1.02(3)	1.0(3)	17(5)
*R*21	1529.836643(10)	0.071(2)	−1.21(3)	1.4(3)	24(5)
*R*18	1531.275090(10)	0.085(2)	−1.45(3)	2.2(3)	38(4)
*R*15	1532.801111(10)	0.085(2)	−1.44(3)	3.2(2)	55(4)
*R*12	1534.414943(10)	0.058(2)	−0.98(3)	4.3(2)	73(3)
*R*10	1535.539723(10)	0.026(2)	−0.45(3)	4.9(2)	83(3)
*R*9	1536.116809(10)	0.005(1)	−0.09(2)	5.0(2)	85(3)
*R*8	1536.703707(22)	−0.021(6)	0.35(9)	5.1(1)	87(2)
*R*7	1537.300409(27)	−0.034(7)	0.58(12)	5.1(1)	86(2)
*R*5	1538.523322(11)	−0.083(2)	1.39(3)	4.8(2)	81(3)
*R*3	1539.785605(12)	−0.111(2)	1.87(4)	4.0(2)	67(3)
*R*1	1541.087342(10)	−0.092(2)	1.55(3)	3.0(2)	50(3)
*R*0	1541.753026(11)	−0.066(2)	1.12(3)	2.6(2)	44(4)
*P*1	1543.114083(10)	0.043(2)	−0.72(3)	2.6(3)	44(4)
*P*4	1545.230028(10)	0.091(2)	−1.52(3)	4.0(2)	68(3)
*P*5	1545.955208(10)	0.084(2)	−1.40(3)	4.5(1)	76(2)
*P*9	1548.955546(11)	0.001(2)	−0.02(3)	5.4(1)	90(2)
*P*10	1549.730587(10)	−0.024(1)	0.40(2)	5.3(1)	89(2)
*P*11	1550.515630(11)	−0.050(2)	0.82(3)	5.2(1)	86(2)
*P*14	1552.930882(14)	−0.112(3)	1.86(4)	4.3(2)	71(3)
*P*16	1554.591255(16)	−0.139(3)	2.30(6)	3.5(2)	59(3)
*P*17	1555.436539(12)	−0.146(2)	2.41(3)	3.2(2)	52(3)
*P*20	1558.032905(22)	−0.151(5)	2.49(9)	2.2(3)	36(5)
*P*23	1560.720279(11)	−0.134(2)	2.19(3)	1.4(3)	23(4)
*P*24	1561.636345(10)	−0.126(2)	2.06(3)	1.2(2)	19(4)

[a]Results are for the measured lines of the $2\nu_3$ band of hydrogen cyanide $H^{13}C^{14}N$ at a temperature of 22° ± 2 °C. The line center vacuum wavelength results are for low-pressure conditions; our measurements (column 2) are values obtained by extrapolating the line center to zero pressure. The broadening coefficient is the pressure dependence of the FWHM of the Lorentzian component of the Voigt line profile. The uncertainties in the final digits of the values are indicated in parentheses. The uncertainties quoted are the expanded uncertainties obtained by applying a coverage factor $k=2$ (i.e., our quoted uncertainty is $\pm 2\sigma$).

sure shift and pressure-broadening determinations. Our zero-pressure line center uncertainty had an additional component due to the wavelength measurement standard uncertainty of 0.004 pm. We combined the wavelength measurement uncertainty with the fit uncertainty using the root-sum-of-squares method to obtain the total uncertainty for the line centers. This analysis resulted in larger uncertainty for the lines identified in Section 2 as having adjacent weak lines (*R*7, *R*8, and *P*20); since the resultant uncertainty for these lines is consistent with our modeling results, we did not add any additional uncertainty due to adjacent lines. Temperature changes affect the collision frequency of molecules in the cell and therefore slightly modify the pressure shift.[1,7] This effect would cause only a 0.2% change of the pressure shift for a 1 °C temperature change.[1] Since the collisional cross section may also have a small temperature dependence (due to small changes of population in the rotational levels, for example), we measured the temperature dependence of line *P*16 and verified that the fractional change of the pressure shift and broadening is small (≤0.3%/°C). We would not expect this temperature dependence to be significantly different for other lines of the spectrum. For the measurements reported here, the temperature was 22° ± 2 °C. This temperature range would have a negligible effect on our pressure shift, broadening, and zero-pressure line center determinations compared with the other sources of uncertainty. Table 1 summarizes our line center, pressure shift, and pressure-broadening results.

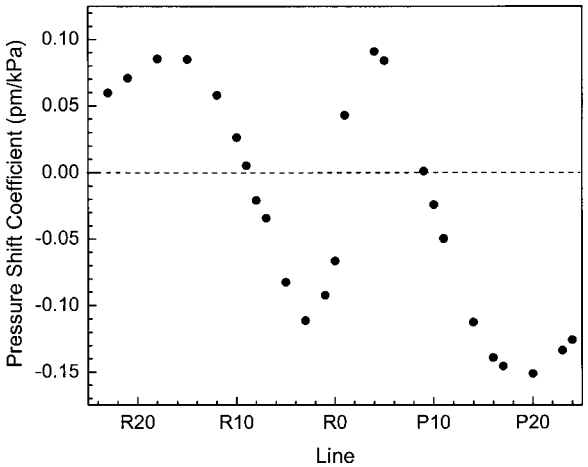

Fig. 5. Measured pressure shift coefficient versus line number for the $H^{13}C^{14}N$ $2\nu_3$ rotational–vibrational band. The error bars are smaller than the data points.

Figure 5 shows the pressure shift versus line number. We find that the pressure shift varies considerably with

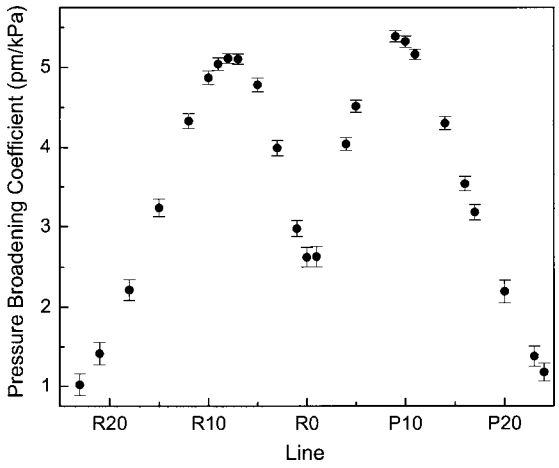

Fig. 6. Measured pressure dependence of the Lorentzian component (FWHM) of the linewidth derived from a Voigt fit versus line number for the $H^{13}C^{14}N$ $2\nu_3$ rotational–vibrational band. Error bars are one standard uncertainty (1σ).

Table 2. Line Center Vacuum Wavelength Measurement Comparison[a]

Line	This Paper Line Center Extrapolated to Zero Pressure (nm)	Ref. 6 (nm)	Difference (pm)
*R*23	1528.92623(1)	1528.92582(24)	0.42(24)
*R*21	1529.83664(1)	1529.83632(24)	0.32(24)
*R*18	1531.27509(1)	1531.27487(24)	0.22(24)
*R*15	1532.80111(1)	1532.80095(24)	0.16(24)
*R*12	1534.41494(1)	1534.41481(24)	0.13(24)
*R*10	1535.53972(1)	1535.53962(24)	0.10(24)
*R*9	1536.11681(1)	1536.11669(24)	0.12(24)
*R*8	1536.70371(2)	1536.70360(24)	0.11(24)
*R*7	1537.30041(3)	1537.30031(24)	0.10(24)
*R*5	1538.52332(1)	1538.52322(24)	0.10(24)
*R*3	1539.78561(1)	1539.78552(24)	0.09(24)
*R*1	1541.08734(1)	1541.08724(24)	0.10(24)
*R*0	1541.75303(1)	1541.75292(24)	0.11(24)
*P*1	1543.11408(1)	1543.11398(24)	0.10(24)
*P*4	1545.23003(1)	1545.22993(24)	0.10(24)
*P*5	1545.95521(1)	1545.95512(24)	0.09(24)
*P*9	1548.95555(1)	1548.95547(24)	0.07(24)
*P*10	1549.73059(1)	1549.73051(24)	0.08(24)
*P*11	1550.51563(1)	1550.51556(24)	0.07(24)
*P*14	1552.93088(1)	1552.93082(24)	0.07(24)
*P*16	1554.59126(2)	1554.59121(24)	0.04(24)
*P*17	1555.43654(1)	1555.43650(24)	0.04(24)
*P*20	1558.03291(2)	1558.03288(24)	0.03(24)
*P*23	1560.72028(1)	1560.72024(24)	0.04(24)
*P*24	1561.63635(1)	1561.63632(24)	0.03(24)

[a]Line center vacuum wavelength results for this measurement compared with those from Ref. 6 for low-pressure conditions; our measurements (column 2) are values obtained by extrapolating the line center to zero pressure. The expanded uncertainties (2σ) in the final digits of the values are indicated in parentheses. We assumed that the uncertainties given in Ref. 6 are one standard uncertainty and we multiplied them by 2.

line number, from approximately +0.09 pm/kPa to −0.15 pm/kPa (approximately −1.5 to +2.5 MHz/Torr). We found that the pressure broadening also varied with line number (Fig. 6). The pressure broadening was largest for the stronger lines in each branch (*R*7, *R*8, *P*9, and *P*10) and is significantly smaller for lines far from the band center (transitions between states with high rotational quantum numbers).

Table 2 compares our determinations of the zero-pressure line center values with the values reported in Ref. 6. Our standard uncertainty (1σ) is typically near 0.005 pm, whereas the estimated uncertainty given in Ref. 6 is 5×10^{-4} cm^{-1} (0.12 pm). With the exception of a deviation in the short-wavelength region (particularly lines *R*21 and *R*23), the results are in good agreement.

We were able to obtain molecular constants for the ground and excited states and determine zero-pressure line center values for other lines in the band by fitting our line center data (converted to cm^{-1}) with the following function:

$$\Delta T_m = \Delta T + B'(m^2+m) - D'(m^2+m)^2 + H'(m^2+m)^3 - B''(m^2-m) + D''(m^2-m)^2 - H''(m^2-m)^3. \quad (2)$$

The index $m=J+1$ for the *R* branch, and $m=-J$ for the *P* branch, where *J* is the ground-state rotational quantum number; ΔT_m is the *m*th line center wavenumber and ΔT is the wavenumber of the pure vibrational transition (band origin). The molecular constants B' and B'' are the excited- and ground-state rotational constants, respectively; and D', D'', H', and H'' are the corresponding centrifugal distortion constants.[9,15] Figure 7 shows the fit to the data and the residuals. The reduced residual-sum-of-squares (χ^2) value for the fit is 0.5, which suggests that we overestimated our uncertainties. Table 3 shows the molecular constants returned by the fit, as well as a comparison of our results with those of Refs. 6 and 16. The line centers of lines *R*0–*R*27 and *P*1–*P*28, calculated from the molecular constants, are listed in Table 4.

Comparison of our results with those of Ref. 16 shows agreement to within our 1σ uncertainties for the ground-state constants (B'', D'', and H''). Our results also agree well with those reported in Ref. 6 for B' and B'', but have poor agreement for ΔT, D', and D''. The value of D'' in Ref. 6 also disagrees with that determined in Ref. 16 by approximately the same amount. The line center results in Ref. 6 are lower than ours by 0.1 pm on average, which led to the 4×10^{-4} cm^{-1} (0.1 pm) discrepancy between

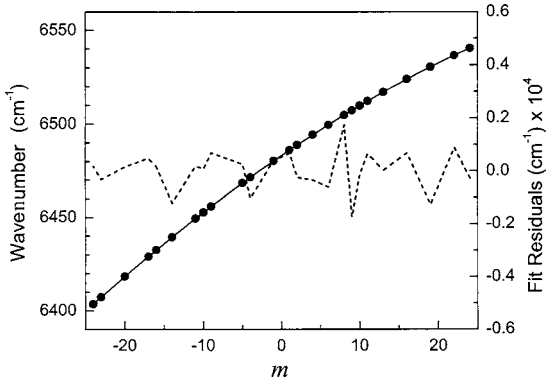

Fig. 7. Zero-pressure line centers (data points), results of fit to Eq. (2) (solid line), and residuals of the fit (dashed curve). The index $m=J+1$ for the *R* branch, and $m=-J$ for the *P* branch. The molecular constants determined by this fit are given in Table 3.

their value for ΔT and ours. The authors in Ref. 6 conducted only high-accuracy measurements (0.0005 cm^{-1} or 0.12 pm uncertainty) of lines $P23$–$P30$ of the $2\nu_3$ band of $H^{13}C^{14}N$ and used lower-accuracy measurements for the remainder of the band in their determination of the molecular constants. As can be seen in Table 2, our line center values are in excellent agreement with those of Ref. 6 for lines with high J values in the P branch, but the agreement progressively deteriorates for lines that are further away from this region.

4. DISCUSSION

We have measured the line centers, pressure shift coefficients, and pressure-broadening coefficients for 25 lines of the $2\nu_3$ rotational–vibrational band of hydrogen cyanide $H^{13}C^{14}N$. We find that the pressure shift varies considerably with line number, from approximately +0.09 pm/kPa to −0.15 pm/kPa (approximately −1.5 to +2.5 MHz/Torr). The pressure broadening also varies with line

Table 3. Molecular Constants for $H^{13}C^{14}N$[a]

Constant	This Work (cm^{-1})	Ref. 16	Difference	Ref. 6	Difference
ΔT	6483.28225(2)	—	—	6483.28267(18)	−0.00042(18)
B'	1.42045356(27)	—	—	1.42045300(46)	$5.6(53)\times10^{-7}$
D'	$2.7225(9)\times10^{-6}$	—	—	$2.7039(26)\times10^{-6}$	$1.9(3)\times10^{-8}$
H'	$3.3(9)\times10^{-12}$	—	—	—	—
B''	1.44000029(27)	1.44000046(4)	$-1.7(27)\times10^{-7}$	1.44000020(22)	$0.9(35)\times10^{-7}$
D''	$2.7684(9)\times10^{-6}$	$2.7682(3)\times10^{-6}$	$2(10)\times10^{-10}$	$2.7525(26)\times10^{-6}$	$1.6(3)\times10^{-8}$
H''	$2.63(90)\times10^{-12}$	$2.66(35)\times10^{-12}$	$-0.03(96)\times10^{-12}$	—	—

[a]Constants were obtained from a fit of our extrapolated zero-pressure line center values to Eq. (2). ΔT is the wavenumber of the pure vibrational transition (band origin). B', D', and H' are the excited-state molecular constants; and B'', D'', and H'' are the ground-state molecular constants. Comparisons with constants reported in Refs. 6 and 16 (converted to cm^{-1}) are also shown. The standard uncertainties (1σ) in the final digits of the values are indicated in parentheses; we assumed that the uncertainties quoted in Ref. 16 are 1σ. Our standard uncertainty for the band origin ΔT includes a 4×10^{-6} cm^{-1} fit uncertainty and a 1.7×10^{-5} cm^{-1} wavelength measurement uncertainty.

Table 4. Calculated Wavenumbers and Vacuum Wavelengths of Line Centers[a]

R Branch	Wavenumber (cm^{-1})	Wavelength (nm)	P Branch	Wavenumber (cm^{-1})	Wavelength (nm)
$R27$	6547.83810(10)	1527.221633(25)	$P1$	6480.40226(3)	1543.114084(8)
$R26$	6546.07370(8)	1527.633273(18)	$P2$	6477.48325(3)	1543.809474(8)
$R25$	6544.26885(6)	1528.054581(13)	$P3$	6474.52527(3)	1544.514784(8)
$R24$	6542.42358(4)	1528.485564(10)	$P4$	6471.52840(3)	1545.230025(8)
$R23$	6540.53793(4)	1528.926231(9)	$P5$	6468.49272(3)	1545.955208(8)
$R22$	6538.61193(4)	1529.376588(8)	$P6$	6465.41828(3)	1546.690341(8)
$R21$	6536.64562(4)	1529.836645(8)	$P7$	6462.30516(3)	1547.435435(8)
$R20$	6534.63904(4)	1530.306408(8)	$P8$	6459.15344(3)	1548.190500(8)
$R19$	6532.59224(4)	1530.785886(8)	$P9$	6455.96319(3)	1548.955548(8)
$R18$	6530.50525(4)	1531.275088(8)	$P10$	6452.73448(3)	1549.730587(8)
$R17$	6528.37812(4)	1531.774020(8)	$P11$	6449.46740(3)	1550.515629(8)
$R16$	6526.21089(4)	1532.282693(8)	$P12$	6446.16201(3)	1551.310685(8)
$R15$	6524.00362(4)	1532.801112(8)	$P13$	6442.81840(3)	1552.115765(8)
$R14$	6521.75633(3)	1533.329289(8)	$P14$	6439.43664(3)	1552.930879(8)
$R13$	6519.46910(3)	1533.867229(8)	$P15$	6436.01682(3)	1553.756039(8)
$R12$	6517.14195(3)	1534.414943(8)	$P16$	6432.55902(3)	1554.591255(8)
$R11$	6514.77496(3)	1534.972439(8)	$P17$	6429.06332(3)	1555.436539(8)
$R10$	6512.36815(3)	1535.539724(8)	$P18$	6425.52981(3)	1556.291901(8)
$R9$	6509.92160(3)	1536.116810(8)	$P19$	6421.95857(4)	1557.157353(8)
$R8$	6507.43535(3)	1536.703703(8)	$P20$	6418.34968(4)	1558.032905(8)
$R7$	6504.90946(3)	1537.300413(8)	$P21$	6414.70324(4)	1558.918569(8)
$R6$	6502.34398(3)	1537.906949(8)	$P22$	6411.01934(3)	1559.814356(8)
$R5$	6499.73898(3)	1538.523321(8)	$P23$	6407.29806(3)	1560.720278(8)
$R4$	6497.09451(3)	1539.149536(8)	$P24$	6403.53949(4)	1561.636345(9)
$R3$	6494.41063(3)	1539.785605(8)	$P25$	6399.74373(4)	1562.562569(10)
$R2$	6491.68740(3)	1540.431537(8)	$P26$	6395.91087(5)	1563.498962(13)
$R1$	6488.92489(3)	1541.087341(8)	$P27$	6392.04100(7)	1564.445534(18)
$R0$	6486.12315(3)	1541.753028(8)	$P28$	6388.13423(10)	1565.402298(25)

[a]Line centers between $R27$ and $P28$ are calculated from the molecular constants returned by the fit to Eq (2). The uncertainties in the final digit of the values are indicated in parentheses. The uncertainties are combined expanded uncertainties (2σ) that include our wavelength uncertainty (8×10^{-6} nm) and the molecular constants fit uncertainty (typically 2×10^{-6} nm).

number and is typically between 1 and 5.4 pm/kPa (17–90 MHz/Torr); the broadening was largest on the stronger lines of each branch. We determined the line centers of the majority of these lines with an expanded uncertainty (2σ) of 0.01 pm ($\approx$1 MHz), an improvement by more than an order of magnitude over previous line center measurements of this band. We also determined the ground- and excited-state molecular constants for the band, yielding improved results for the band origin and excited-state molecular constants.

Our pressure shift and broadening measurements of $H^{13}C^{14}N$ show significantly different trends compared with our results for acetylene[1] and carbon monoxide.[4] This is not surprising since HCN is a strongly polar molecule and hence long-range dipole–dipole interactions dominate the collisional process. The Boltzmann-like distribution of the broadening coefficients has been noted in previous work.[17] The authors in Ref. 17 conclude that rotationally resonant dipole collisions, where one molecule goes from J to $J+1$ and the other from $J+1$ to J, have large cross sections in HCN and dominate the pressure broadening. The strong asymmetry of the pressure shift between the R and P branches and changes in sign that we observe here have also been observed in hydrogen fluoride and are analyzed in Ref. 18 in the framework of the impact approximation with an expansion of the S matrix to second order with respect to the intermolecular potential energy. The authors conclude that the sign of the shift depends on whether the first- or second-order term dominates.

ACKNOWLEDGMENTS

We gratefully acknowledge the help of C. Wang for discussions and suggestions on the uncertainty analysis and D. Franzen and R. Fox for discussions and comments on the manuscript.

REFERENCES

1. W. C. Swann and S. L. Gilbert, "Pressure-induced shift and broadening of 1510–1540-nm acetylene wavelength calibration lines," J. Opt. Soc. Am. B **17**, 1263–1270 (2000).
2. S. L. Gilbert and W. C. Swann, "Acetylene $^{12}C_2H_2$ absorption reference for 1510 nm to 1540 nm wavelength calibration—SRM 2517a," Natl. Inst. Stand. Technol. (US) Spec. Publ. 260-133 (National Institute of Standards and Technology, 2001).
3. S. L. Gilbert, W. C. Swann, and C. M. Wang, "Hydrogen cyanide $H^{13}C^{14}N$ absorption reference for 1530–1560 nm wavelength calibration—SRM 2519," Natl. Inst. Stand. Technol. (US) Spec. Publ. 260-137 (National Institute of Standards and Technology, 1998).
4. W. C. Swann and S. L. Gilbert, "Pressure-induced shift and broadening of 1560–1630-nm carbon monoxide wavelength calibration lines," J. Opt. Soc. Am. B **19**, 2461–2467 (2002).
5. S. L. Gilbert and W. C. Swann, "Carbon monoxide absorption references for 1560 nm to 1630 nm wavelength calibration—SRM 2514 ($^{12}C^{16}O$) and SRM 2515 ($^{13}C^{16}O$)," Natl. Inst. Stand. Technol. (US) Spec. Publ. 260-146 (National Institute of Standards and Technology, 2002).
6. H. Sasada and K. Yamada, "Calibration lines of HCN in the 1.5-μm region," Appl. Opt. **29**, 3535–3547 (1990).
7. W. Demtröder, *Laser Spectroscopy*, 2nd ed. (Springer-Verlag, 1996), pp. 67–82.
8. P. A. Boggs, R. H. Byrd, J. E. Rogers, and R. B. Schnabel, "Users reference guide for ODRPAC version 2.01 software for weighted orthogonal distance regression," Natl. Inst. Stand. Technol. (US) Interagency Rep. 4834 (National Institute of Standards and Technology, 1992).
9. K. Nakagawa, M. de Labachelerie, Y. Awaji, and M. Kourogi, "Accurate optical frequency atlas of the 1.5-μm bands of acetylene," J. Opt. Soc. Am. B **13**, 2708–2714 (1996).
10. P. L. Varghese and R. K. Hanson, "Collisional narrowing effects on spectral line shapes measured at high resolution," Appl. Opt. **23**, 2376–2385 (1984).
11. B. N. Taylor and C. E. Kuyatt, "Guidelines for evaluating and expressing the uncertainty of NIST measurement results," Natl. Inst. Stand. Technol. (US) Tech. Note 1297 (National Institute of Standards and Technology, 1993).
12. G. P. Barwood, P. Gill, and W. R. C. Rowley, "Frequency measurements on optically narrowed Rb-stabilized laser diodes at 780 nm and 795 nm," Appl. Phys. B **53**, 142–147 (1991).
13. J. Ye, S. Swartz, P. Jungner, and J. L. Hall, "Hyperfine structure and absolute frequency of the ^{87}Rb $5P_{3/2}$ state," Opt. Lett. **21**, 1280–1282 (1996).
14. K. L. Corwin, I. Thomann, T. Dennis, R. W. Fox, W. Swann, E. A. Curtis, C. W. Oates, G. Wilpers, A. Bartels, S. L. Gilbert, L. Hollberg, N. R. Newbury, S. A. Diddams, J. W. Nicholson, and M. F. Yan, "Absolute frequency measurements with a stabilized near-infrared optical frequency comb from a Cr:forsterite laser," Opt. Lett. **29**, 397–399 (2004).
15. F. J. Lovas, J. S. Coursey, S. A. Kotochigova, J. Chang, K. Olsen, and R. A. Dragoset, Triatomic Spectral Database (version 2.0), http://physics.nist.gov/Triatomic (National Institute of Standards and Technology, 2003).
16. F. Maiwald, F. Lewen, V. Ahrens, M. Beaky, R. Gendriesch, A. N. Koroliev, A. A. Negirev, D. G. Paveljev, B. Vowinkel, and G. Winnewisser, "Pure rotational spectrum of HCN in the terahertz region: use of a new planar Schottky diode multiplier," J. Mol. Spectrosc. **202**, 166–168 (2000).
17. A. M. Smith, K. K. Lehmann, and W. Klemperer, "The intensity and self-broadening of overtone transitions in HCN," J. Chem. Phys. **85**, 4958–4965 (1986).
18. C. Boulet, D. Robert, and L. Galatry, "Shifts of the vibration-rotation absorption line of diatomic molecules perturbed by diatomic polar molecules. A theoretical analysis," J. Chem. Phys. **65**, 5302–5314 (1976).